SANDIA REPORT

SAND2013-9863
Unlimited Release
Printed November 2013

Investigations of Shot Reproducibility for the SMP Diode at 4.5 MV

Nichelle Bennett, Steve Cordova, Marlon D. Crain, Darryl W. Droemer, Raymond Cignac, Mark D. Johnston, Mark L. Kiefer, Greg Lare, Josh Leckbee, Isidro Molina, Dan Nielsen, Robert Obregon, Brian V. Oliver, Timothy Renk, Tobias Romero, Chase Smith, Timothy Webb, Dale R. Welch, Frank Wilkins, Derek Ziska

Prepared by
Sandia National Laboratories
Albuquerque, New Mexico 87185 and Livermore, California 94550

Sandia National Laboratories is a multi-program laboratory managed and operated by Sandia Corporation, a wholly owned subsidiary of Lockheed Martin Corporation, for the U.S. Department of Energy's National Nuclear Security Administration under contract DE-AC04-94AL85000.

Approved for public release; further dissemination unlimited.

Sandia National Laboratories

Issued by Sandia National Laboratories, operated for the United States Department of Energy by Sandia Corporation.

NOTICE: This report was prepared as an account of work sponsored by an agency of the United States Government. Neither the United States Government, nor any agency thereof, nor any of their employees, nor any of their contractors, subcontractors, or their employees, make any warranty, express or implied, or assume any legal liability or responsibility for the accuracy, completeness, or usefulness of any information, apparatus, product, or process disclosed, or represent that its use would not infringe privately owned rights. Reference herein to any specific commercial product, process, or service by trade name, trademark, manufacturer, or otherwise, does not necessarily constitute or imply its endorsement, recommendation, or favoring by the United States Government, any agency thereof, or any of their contractors or subcontractors. The views and opinions expressed herein do not necessarily state or reflect those of the United States Government, any agency thereof, or any of their contractors.

Printed in the United States of America. This report has been reproduced directly from the best available copy.

Available to DOE and DOE contractors from
U.S. Department of Energy
Office of Scientific and Technical Information
P.O. Box 62
Oak Ridge, TN 37831

Telephone: (865) 576-8401
Facsimile: (865) 576-5728
E-Mail: reports@adonis.osti.gov
Online ordering: http://www.osti.gov/bridge

Available to the public from
U.S. Department of Commerce
National Technical Information Service
5285 Port Royal Rd
Springfield, VA 22161

Telephone: (800) 553-6847
Facsimile: (703) 605-6900
E-Mail: orders@ntis.fedworld.gov
Online ordering: http://www.ntis.gov/help/ordermethods.asp?loc=7-4-0#online

SAND2013-9863
Unlimited Release
Printed November 2013

Investigations of Shot Reproducibility for the SMP Diode at 4.5 MV

N. Bennett, M.D. Crain, D.W. Droemer, R. Gignac, G. Lare,
I. Molina, R. Obregon, C. Smith, and F. Wilkins
National Security Technologies, LLC, Las Vegas, NV 89193

D.R. Welch
Voss Scientific, LLC, Albuquerque, NM 87108

S. Cordova, M. Gallegos, M.D. Johnston, M.L. Kiefer, J.J. Leckbee, D. Nielsen,
B.V. Oliver, T.J. Renk, T. Romero, T.J. Webb, and D. Ziska
Sandia National Laboratories,Albuquerque, NM 87185

Abstract

In experiments conducted on the RITS-6 accelerator, the SMP diode exhibits significant shot-to-shot variability. Specifically, for identical hardware operated at the same voltage, some shots exhibit a catastrophic drop in diode impedance. A study is underway to identify sources of shot-to-shot variations which correlate with diode impedance collapse. To remove knob emission as a source, only data from a shot series conducted with a 4.5-MV peak voltage are considered. The scope of this report is limited to sources of variability which occur away from the diode, such as power flow emission and trajectory changes, variations in pulsed power, dustbin and transmission line alignment, and different knob shapes. We find no changes in the transmission line hardware, alignment, or hardware preparation methods which correlate with impedance collapse. However, in classifying good versus poor shots, we find that there is not a continuous spectrum of diode impedance behavior but that the good and poor shots can be grouped into two distinct impedance profiles. This result forms the basis of a follow-on study focusing on the variability resulting from diode physics.

Acknowledgments

This work was conducted by National Security Technologies, LLC, under Contract No. DE-AC52-06NA25946 with the U.S. Department of Energy.

Contents

1 Introduction . . . 7
2 Identifying poor radiographic shots . . . 9
3 MITL electron emission thresholds . . . 12
3.1 Simulation details . . . 12
3.2 Shots at 3.5 MV . . . 14
3.3 Shots at 4.5 MV . . . 15
4 Pulsed power correlation to poor shots . . . 18
5 Dustbin and MITL alignment correlation to poor shots . . . 20
6 Knob hardware correlation to poor shots . . . 22
7 Diode impedance collapse characteristics . . . 23
8 Diode current comparison to theory . . . 27
9 Conclusion . . . 31

1 Introduction

Radiation pulse reproducibility is critically important for the radiographic sources under development at Sandia National Laboratories. To determine the suitability of the self-magnetic-pinch (SMP) diode [1] as a radiographic source, an experimental campaign was conducted on Sandia's RITS-6 accelerator to quantify its shot-to-shot variation. The accelerator operated at 4.5 MV and the SMP diode was fielded with changes only to the anode-cathode (AK) gap and cathode needle radius (r_c). We refer to a diode geometry by the needle diameter and AK gap width, such that a 7-mm-diameter cathode fielded with a 7-mm AK gap width is a *7-7* shot.

Variations in SMP diode performance occur in spot size, pulse width, and impedance lifetime. In normal operation, this diode has a decreasing impedance related to anode plasma expansion [2]. Occasionally this diode experiences a more rapid impedance drop ($> 0.5\ \Omega/\text{ns}$) resulting in a radiographically poor shot. We wish to identify sources of shot variability which correlate with diode impedance collapse.

Possible sources of variation between shots with identical hardware and geometry include

1. power flow emission and trajectory changes,
2. variations in pulsed power,
3. dustbin and transmission line misalignment,
4. different knob shapes,
5. diode misalignment,
6. non-uniform electron emission from the cathode needle,
7. non-uniform emission from the faceplate, and
8. an unidentified plasma-induced impedance collapse mechanisms.

In this report, we examine only the sources which occur away from the diode (the first four).

To address the first two items above, we investigate the possibility of shot-to-shot variations in the electron emission along the magnetically insulated transmission line (MITL). We simultaneously look at the dynamics of power-flow electrons in the dustbin, which are related to variations in emission and to the load impedance. Simulations are used to determine the electric field stress thresholds for electron emission for a sample of shots. The measured forward-going voltage pulses are used as input to the simulations to enable direct comparisons to shot data. Since the simulation of each shot takes four days on 20 processors, the statistics of this analysis are limited. Instead, the shots are sampled from March through August of 2013. The results, presented in Sec. 3, show a stable emission threshold and a consistent pattern of electron flow in the dustbin from shot to shot.

The question of variations in pulsed power may be treated more statistically. In Sec. 4 anode currents in the MITL are compared for 99 shots to determine if poor diode performance is correlated with peak injected power. Poor diode performance is indicated by an above-average reduction in diode impedance, and subsequent rise in the cathode current. The

results show that the anode currents for poor shots, and therefore their peak power, are well-represented by the Gaussian distribution defined by the good shots, until the retrapping wave arrives from downstream. The same result is obtained in a comparison of pulse-rises determined from the anode currents.

The effects of MITL and dustbin alignment are also treated statistically. Misalignment could cause azimuthally asymmetric currents, which might affect the diode. Asymmetries for the MITL and dustbin B-dot probes are calculated and sorted by diode performance in Sec. 5. No correlation is found between the level of azimuthal asymmetry and poor shots.

Of hardware correlations, we found that one of the six knobs fielded is more highly correlated with poor shots. However, as shown in Sec. 6, poor shots are recorded for every knob, so knob type is unlikely the primary cause of impedance collapse.

Poor shots are identified in Sec. 2 by a larger-than-average rise in their cathode currents in the MITL which is a result of lower load impedance. The motivation that this is due to diode impedance collapse is provided in Sec. 7. The diode impedance profiles form a bimodal distribution for good and poor shots.

The diode currents are compared to the theoretical critical current in Sec. 8. We modify this theory to account for a time-dependent AK gap width and calculate a gap closure velocity of approximately $v_p = 1$ cm/μs. The theory is well-matched to data, which exhibit the expected scaling with cathode and AK gap size.

2 Identifying poor radiographic shots

Poor radiographic performance of a diode is the result of the electron beam having a large or wandering focus at the converter, a low diode voltage, or a low usable beam current. When the SMP diode fails, it experiences an increase in local current, either due to a rapid drop in impedance or because it is no longer obeys the standard critical-current equation (see for example Ref.3.) The instability presumably disrupts the beam focus because the radiation output is truncated.

The diode failure is observed upstream as a decrease in load impedance above what is expected for the dustbin/knob and diode geometries. The SMP diode as fielded on RITS-6 is under-matched to the MITL, so some power-flow current is retrapped in the cathode for emission in the diode. The amount of retrapping is much larger when the diode fails. This is easily seen in the currents measured at position F, which is defined in Sec. 3. The anode and cathode currents, OF and IF, are plotted in Figs. 1 and 2 for 76 shots. The diode geometries are labeled in each figure. The cathode current after retrapping differs by geometry, or baseline diode impedance, but is still noticeably larger in poor shots.

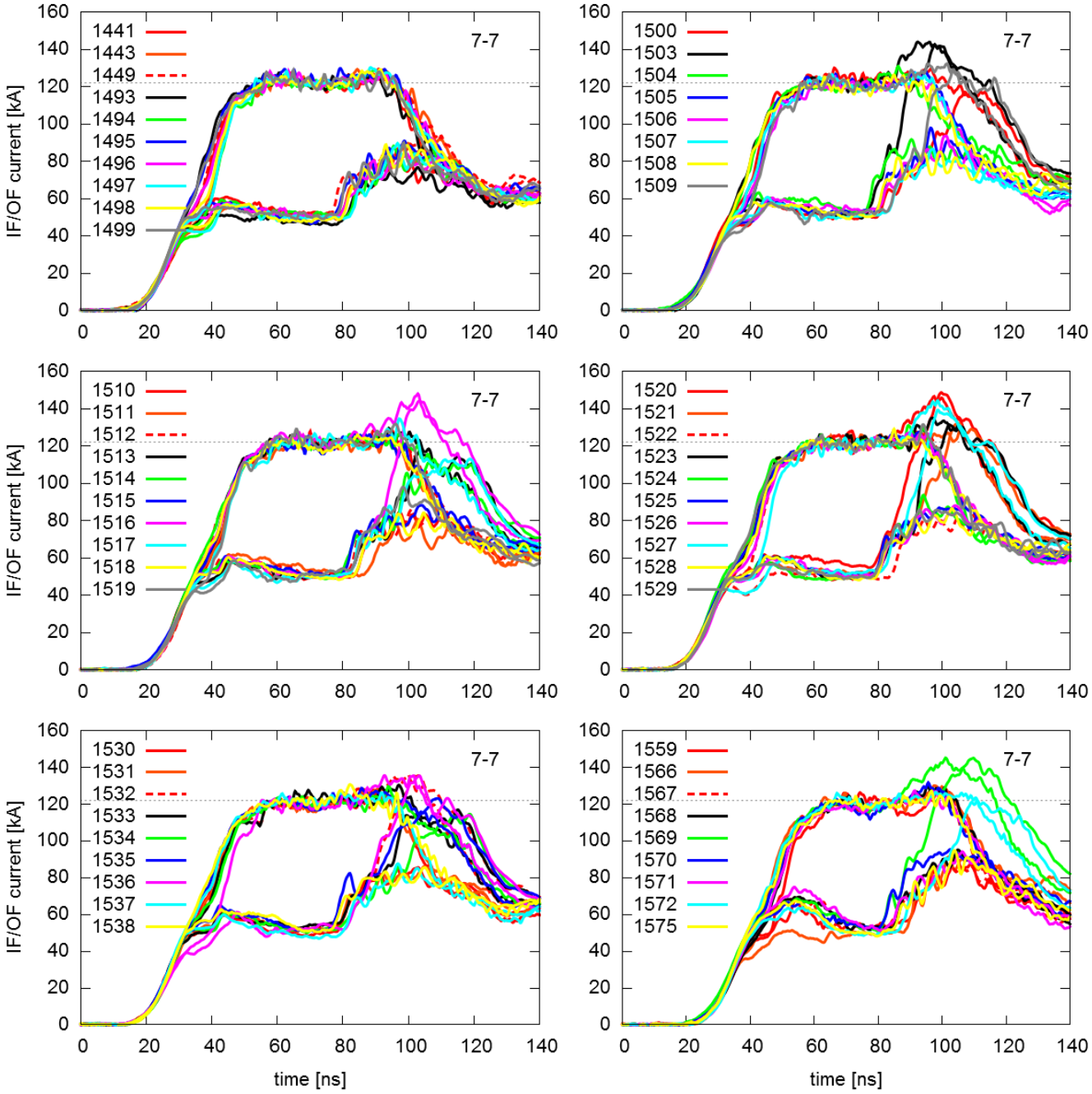

Figure 1. The IF and OF currents for SMP diode shots with a 7-mm diameter cathode needle and a 7-mm AK gap. The gray dotted lines are the average OF in the first 10 ns at peak power.

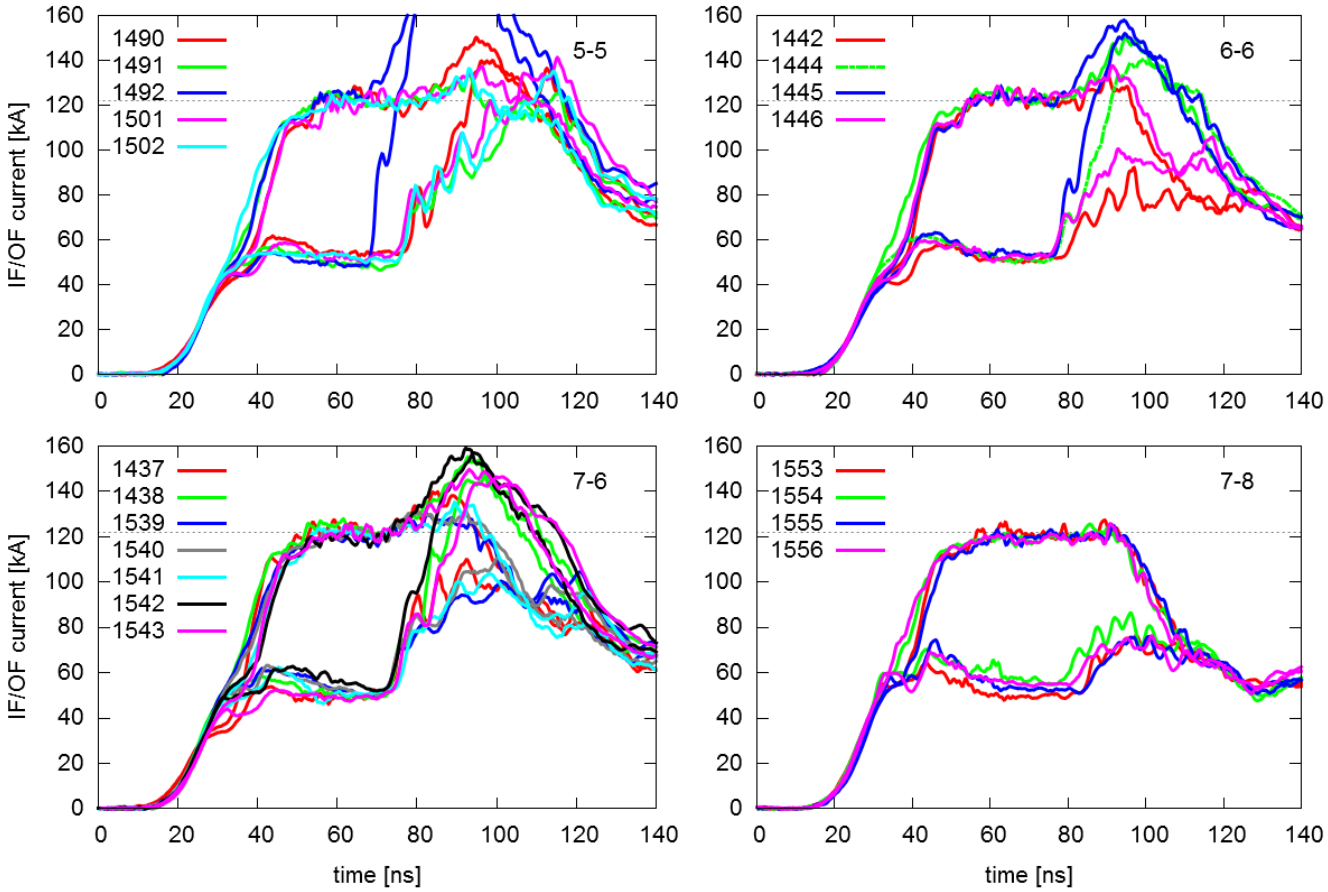

Figure 2. The IF and OF currents for SMP diode shots with various cathode diameters and AK gap widths. Top left is the 5-mm diameter cathode and 5-mm AK gap. Top right is the 6-mm diameter cathode and 6-mm AK gap. The bottom left and right have 7-mm AK gaps with a 6-mm and 8-mm diameter cathode, respectively. The gray dotted lines are the average OF in the first 10 ns at peak power.

3 MITL electron emission thresholds

Simulations are performed of specific shots to determine the operating conditions of the MITL, dustbin, and knob. For each shot considered, the forward-going voltage calculated at position F is used as the injected voltage wave in its corresponding simulation. The simulation parameters, such as electron emission thresholds, are adjusted to achieve the best match to the measured B-dot currents at five locations. Variations in these model parameters from simulation to simulation indicate shot-to-shot variations in the transmission line and dustbin. Since measured voltages are used as input, variations in the pulse driver are not considered.

The B-dot probe positions analyzed are

IF and OF The inner and outer currents at position F, located 1.16 m upstream from the dustbin entrance.

IFEED The cathode current immediately upstream from the knob.

IBEAM The cathode current inside a 6.35-cm radius on the knob face plate. This includes the beam current and a limited region of possible knob emission.

DIODB The anode current inside an 11-cm radius on the end plate.

Using a single set of emission thresholds for all simulations, the currents are all in reasonable agreement with their respective shot data, shown in detail in Secs. 3.2 and 3.3. This uniformity is significant because even a 5% change in the emission threshold in the MITL caused a noticeable change in cathode current. Therefore, the MITL conditions (cleaning process, application of Aerodag, alignment) appears consistent from shot to shot.

To achieve agreement between simulations and data, emission thresholds are adjusted based on location in the transmission line (see Sec. 3.1). For example, to achieve the correct boundary current profile at position F, the cathode must emit earlier downstream than upstream. This is consistent with the location of pump-out ports in the cathode. The onset of emission at position F, the electron flow trajectory in the dustbin, and the retrapping rate on the knob are well modeled. The results from a 3.5-MV simulation are presented in Sec. 3.2. The results from 4.5-MV simulations are presented in Sec. 3.3. One of thees shots exhibits impedance collapse after which it no longer agrees with simulation.

3.1 Simulation details

All simulations are performed in 2D cylindrical coordinates using the fully-relativistic electromagnetic particle-in-cell code Lsp [4]. All simulations have the same geometry, covering the dustbin region and 1.7 m of the MITL upstream of the dustbin. The common simulation geometry is illustrated in Fig. 3. The accelerator cavities are omitted so that measured

forward-going voltage pulses may be used to drive the simulations. This enables direct comparisons between currents generated in simulations and data.

In Fig. 3, the dustbin covers $166 < z < 257$ cm and the knob is located from $z = 197.5$ cm to $z = 222.5$ cm. The sub-cell model is used for the knob to reduce the effect of field enhancement due to the stair-stepped representation of the curved surface. Probe position F is located at $z = 50.0$ cm, IFEED is at $z = 197.5$ cm, IBEAM is at (6.35, 222.65) and DIODB is at (11.0, 257.0).

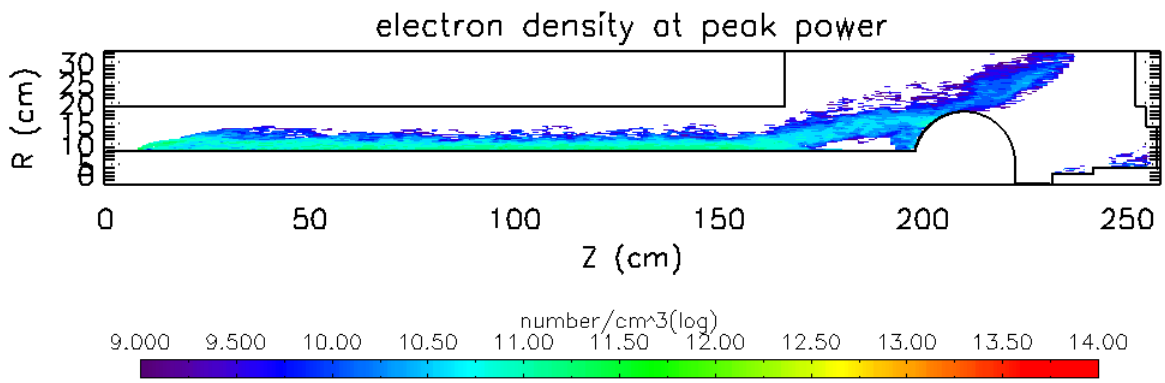

Figure 3. Simulation geometry of the RITS-6 accelerator front end, including the dustbin and diode. Contours of the power-flow electron density at peak power are also shown on a log scale.

The diode is modeled with the actual SMP diode dimensions fielded, but with the minimum resolution required to provide a realistic value of the IBEAM current. The spatial resolution in the diode region is 200 μm, which enables modeling of anode heating and bipolar flow. Plasma effects are not included and, instead, a simplified model of fluid particles is used to generate the falling diode impedance, if needed. In this model, massive electrons are injected from the anode surface after the pulse rise in order to attract a portion of the emitted ions. These electrons drift toward the cathode at 1 cm/μs and, with accompanying ions, carry the anode potential into the AK gap, approximating an expanding anode plasma. After the initial "turn-on", the electron injection continues at the anode surface, increasing the plasma density. The appearance of the massive electrons at the anode interferes with the beam focus, however, so spot size and dose rate probes are not considered.

The first shot modeled was shot 1394, an *8-8* diode. To achieve the best match to this shot, the emission threshold in the MITL is 280 kV/cm over $0 < z < 115$ cm and 100 kV/cm over $115 < z < 198.5$ cm. This change in threshold approximates the effect of pump-out ports near position G. The knob emission threshold is 950 kV/cm, although for most simulations 550 kV/cm was sufficient to prevent knob emission. Electrons are emitted from the cathode needle above 100 kV/cm, or 40 kV/cm where silver paint is applied.

3.2 Shots at 3.5 MV

One shot is modeled at the 3.5-MV end-point voltage. This is shot 1394 which has an *8-8* diode geometry. The simulated currents are compared to data in Fig. 4. All currents have smoothing applied, so no conclusion should be drawn regarding the magnitude of oscillations. The measured pulses are shifted in time so that IF and OF are aligned at the pulse rise. The other currents use this time shift.

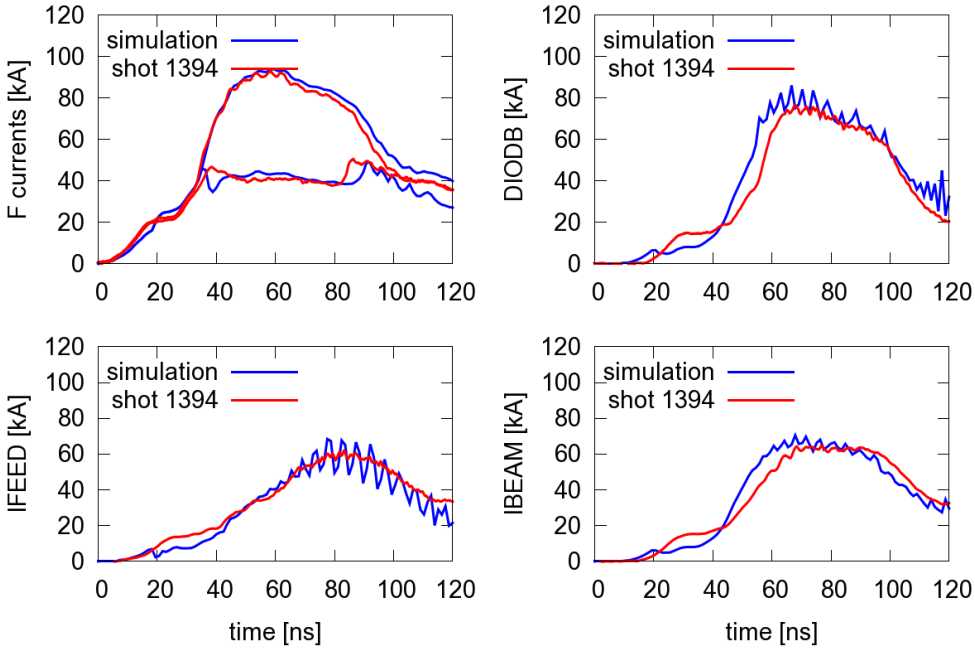

Figure 4. Currents in the MITL, dustbin, and diode from a simulation of shot 1394 compared to data. The diode has a 8-mm diameter needle and a 8-mm AK gap. The diode impedance in the simulation is stable.

The retrapping speed on the knob is well-matched, based on IFEED. Since DIODB equals IBEAM during the pulse rise, the power flow electrons are impacting the dustbin wall at larger radius. The rise in beam current is faster in simulation than data, and this causes the disagreement during the pulse rise for IBEAM and DIODB. The measured diode currents for all shots appear to turn-on rapidly in the first 10 ns and then relax to a more gradual rise. We do not attempt to model this effect.

3.3 Shots at 4.5 MV

A few shots are modeled for the 4.5-MV end-point voltage (1441, 1509, 1519). Each uses the 7-7 geometry but all have different diode impedance lifetimes. The massive-fluid-electron model is used in each simulation to achieve the falling diode impedance seen in the IBEAM current.

The comparison to shot 1441 is shown in Fig. 5. A snapshot of the electron density in the MITL power flow for this simulation is shown in Fig. 3. The start time and rate of injection of massive electrons at the anode surface was adjusted to match the measured gap closure. The comparisons to shots 1509 and 1519 are shown in Figs. 6 and 7, respectively.

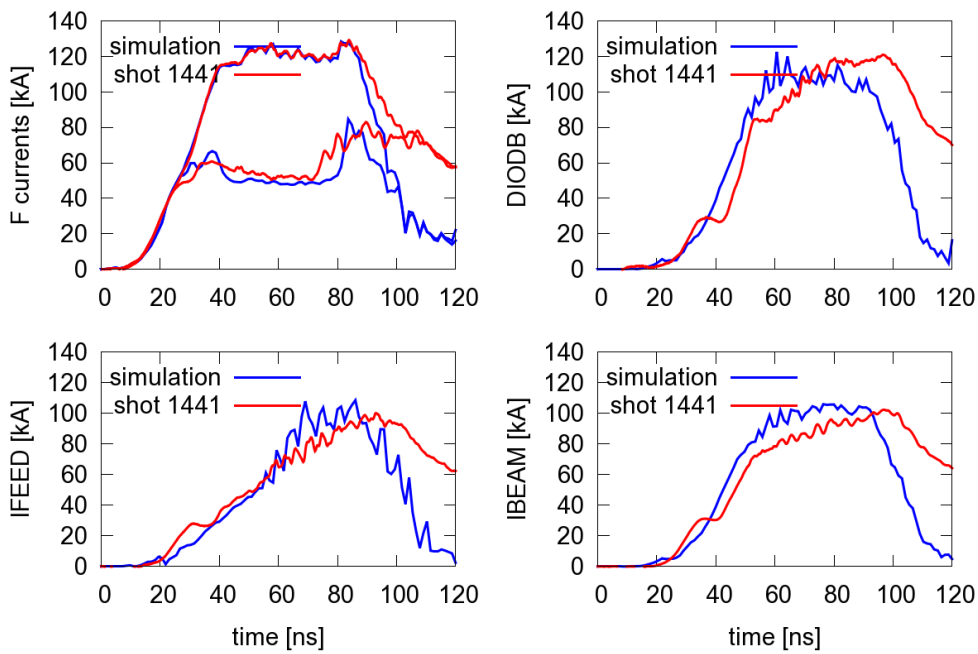

Figure 5. Currents in the MITL, dustbin, and diode from a simulation of shot 1441 compared to data. The diode has a 7-mm diameter needle and a 7-mm AK gap.

Comparing the IBEAM currents in Figs. 5, 6 and 7, we see a rapid decrease in diode impedance in shot 1509. This shot begins identically to the others, but at approximately 30 ns into peak power, the diode current increases more rapidly. The reproducibility of the diode impedance profiles is examined statistically in Sec. 7. The theory of the pre-collapse behavior is examined in Sec. 8.

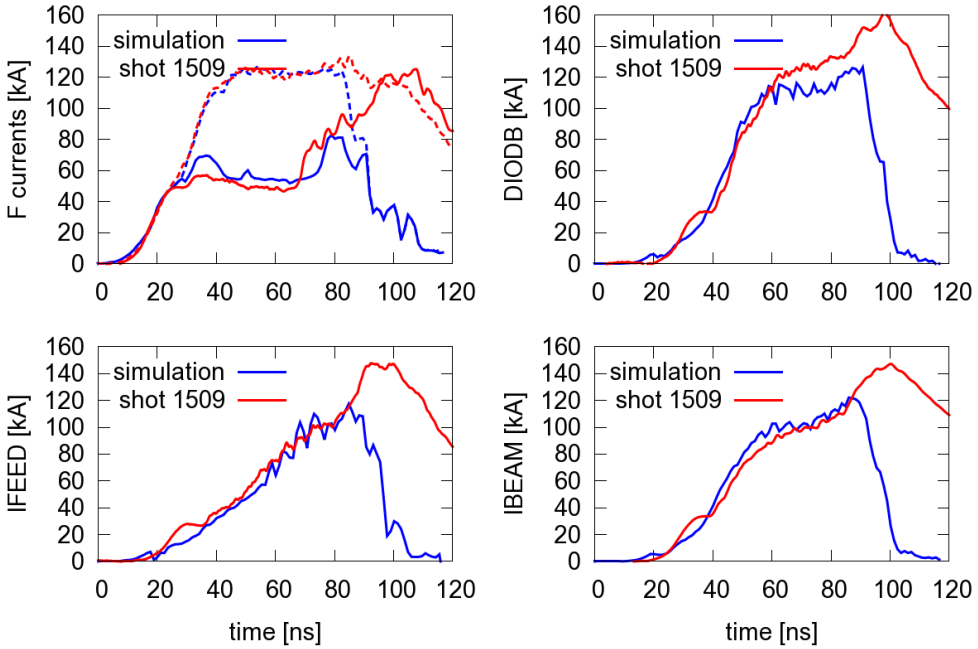

Figure 6. Currents in the MITL, dustbin, and diode from a simulation of shot 1509 compared to data. The diode has a 7-mm diameter needle and a 7-mm AK gap. The falling diode impedance is modeled using massive fluid electrons at the anode which drift away from the surface and effectively reduce the AK gap.

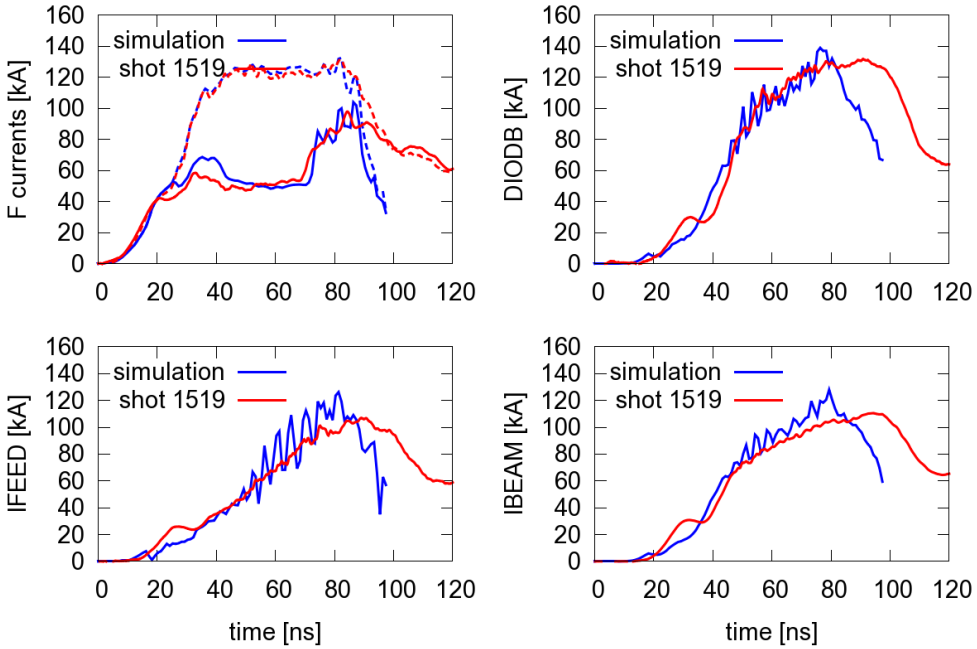

Figure 7. Currents in the MITL, dustbin, and diode from a simulation of shot 1519 compared to data. The diode has a 7-mm diameter needle and a 7-mm AK gap. The falling diode impedance is modeled using massive fluid electrons at the anode which drift away from the surface and effectively reduce the AK gap.

4 Pulsed power correlation to poor shots

Variations in injected power could manifest as differences in peak power or pulse rise, and these could impact power-flow current uniformity or insulation. To determine if variations in peak power correlate with poor performing shots, we plot the peak anode current versus shot number for 99 shots in Fig. 8, noting which are good and poor. The peak anode current is calculated by taking the average value at OF during the first 10 ns of peak power. (Position F is far enough from the load that impedance feedback, in the form of a retrapping wave, arrives during the second half of the pulse.) The average peak current is represented by a solid gray line and the standard deviation is indicated with dotted lines.

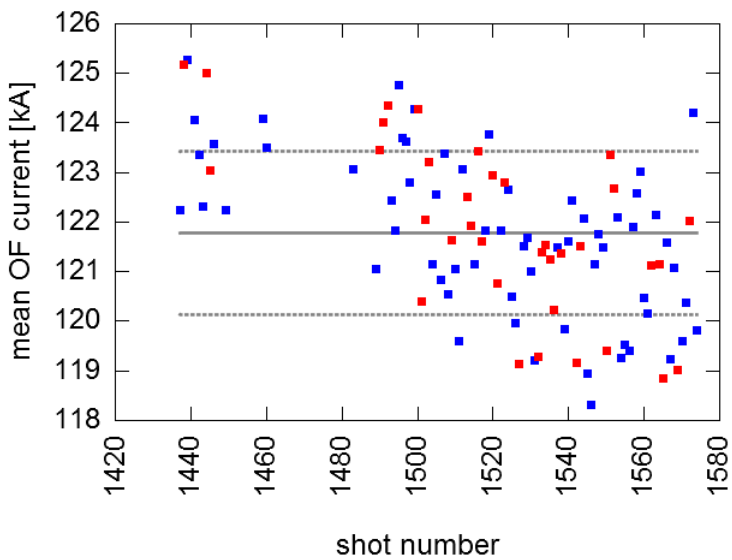

Figure 8. The magnitude of the OF current at peak power versus shot number. Good shots are shown in blue and poor shots in red. The values shown are averaged over the first 10 ns at peak power.

The OF currents for poor shots, shown in red in Fig. 8, are are well-represented by a Gaussian distribution defined by the good shots (reduced $\chi^2 = 1.04$) until the retrapping wave arrives from downstream. There appears to be more of a correlation with shot number and peak current than with diode impedance.

The pulse rises for poor shots, shown in red in Fig. 9, are are also well-represented by the Gaussian distribution defined by the good shots (reduced $\chi^2 = 1.27$.)

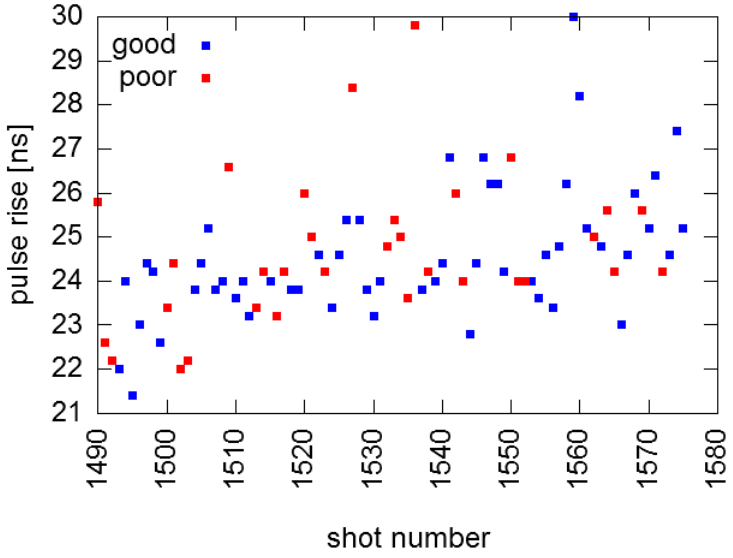

Figure 9. The pulse rise from OF versus shot number. Good shots are shown in blue and poor shots in red. The rise is calculated as the time to rise from 10% to 90% of the mean OF current.

5 Dustbin and MITL alignment correlation to poor shots

If the cathode is misaligned to the anode in the transmission line or dustbin, the power-flow current should become asymmetric around the line or knob. To determine if misalignment is correlated with poor shots, we calculate the asymmetries in the MITL and dustbin currents and plot these values versus shot number, noting good and poor shots.

Each current presented in this report is the average of four B-dot probes arrayed azimuthally at a given axial position (listed in Sec. 3). Azimuthal asymmetry is calculated as the difference between the highest probe value at a given position and the average, normalized by the average, $(I_{max} - \bar{I})/\bar{I}$. This value is calculated for the IFEED and IF probes from 80 shots and plotted versus shot number in Fig. 10. Good shots are shown in blue and poor shots in red. There is no discernible correlation between the level of asymmetry and shot performance. The distributions of the poor shots for IFEED and IF asymmetry are well-represented by Gaussians defined by the good shots (reduced $\chi^2 = 0.73$ and 0.58, respectively.)

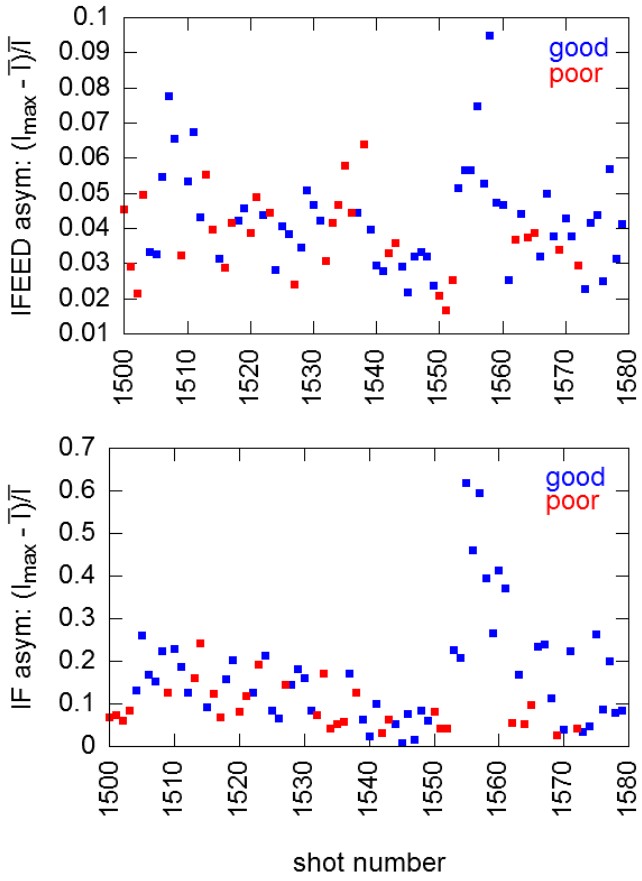

Figure 10. The azimuthal asymmetry of the IFEED (top) and IF (bottom) currents versus shot number. The asymmetry is the difference between the highest probe value and the average, normalized by the average, $(I_{max} - \bar{I})/\bar{I}$. Good shots are shown in blue and poor shots in red.

6 Knob hardware correlation to poor shots

There are six knobs used with the small dustbin, each with slightly different shape. To investigate the possibility that the structure of a subset of these contributes to shot failure, we plot the frequency of good and poor shots for each knob in Fig. 11. While knob #6 has a higher rate of occurrence of poor shots, they occur for every knob. We do not conclude that the shots fail exclusively as a result of a subset of knob hardware.

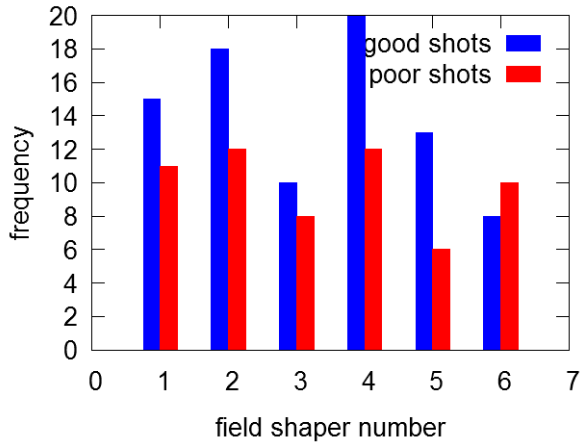

Figure 11. The frequency with which one of six knobs is used on good and poor shots. Good shots are shown in blue and poor shots in red.

7 Diode impedance collapse characteristics

In the compilation of cathode and anode currents (IF and OF) in Sec. 2, poor shots are identified by a larger-than-average rise in IF after the retrapping wave has passed. This is a result of a larger-than-average drop in the load impedance. Since the abnormal current increase is first recorded in the IBEAM probes, the impedance change must be occurring in the diode, and not elsewhere in the dustbin.

In normal operation, the SMP diode has a slowly decreasing impedance ($< 0.5\Omega$/ns) related to anode plasma expansion. This results in a steady rise in the IBEAM currents, after the pulse rise, as shown in Figs. 12 and 13. Initially, the rate of increase is the same for all shots and is related to r_c/g, as discussed in Sec.8. For poor shots, IBEAM increases sharply at some time during peak power. The time to impedance breakdown is different for the shots in this series, but breakdown is never gradual. The drop in impedance is catastrophic, causing the diode to draw the entire line current.

In average operation, the DIODB current is higher than IBEAM after pulse rise. This indicates that some power-flow current is wrapping around the knob and connecting to the anode within an 11-cm radius. (This is the electron density seen on the anode holder in Fig. 3.) In this shot series, when the diode impedance drops abnormally low, IBEAM and DIODB rise to nearly the same value and IF becomes almost equal to OF, indicating that the power flow is recaptured in the cathode and the diode current is almost the total current in the system. This is seen in the IBEAM and DIODB currents for the 7-7 shots in Figs. 12 and 13, and in the IF/OF currents in Figs. 1 and 2.

To quantify how much the power flow is reduced for poor shots, the ratio of DIODB to IBEAM is plotted versus IBEAM in Fig. 14. We see that there are two distinct distributions. For good shots, IBEAM ranges around 100 to 110 kA and DIODB is 16 to 30% larger. For failed shots IBEAM is near 140 to 150 kA and DIODB is usually less than 10% larger. That the distribution is bimodal instead of continuous and involves a significant reduction in power flow strongly suggests that power-flow electrons are not contributing to this catastrophic impedance collapse, but rather this phenomenon is a result of physics in the diode region.

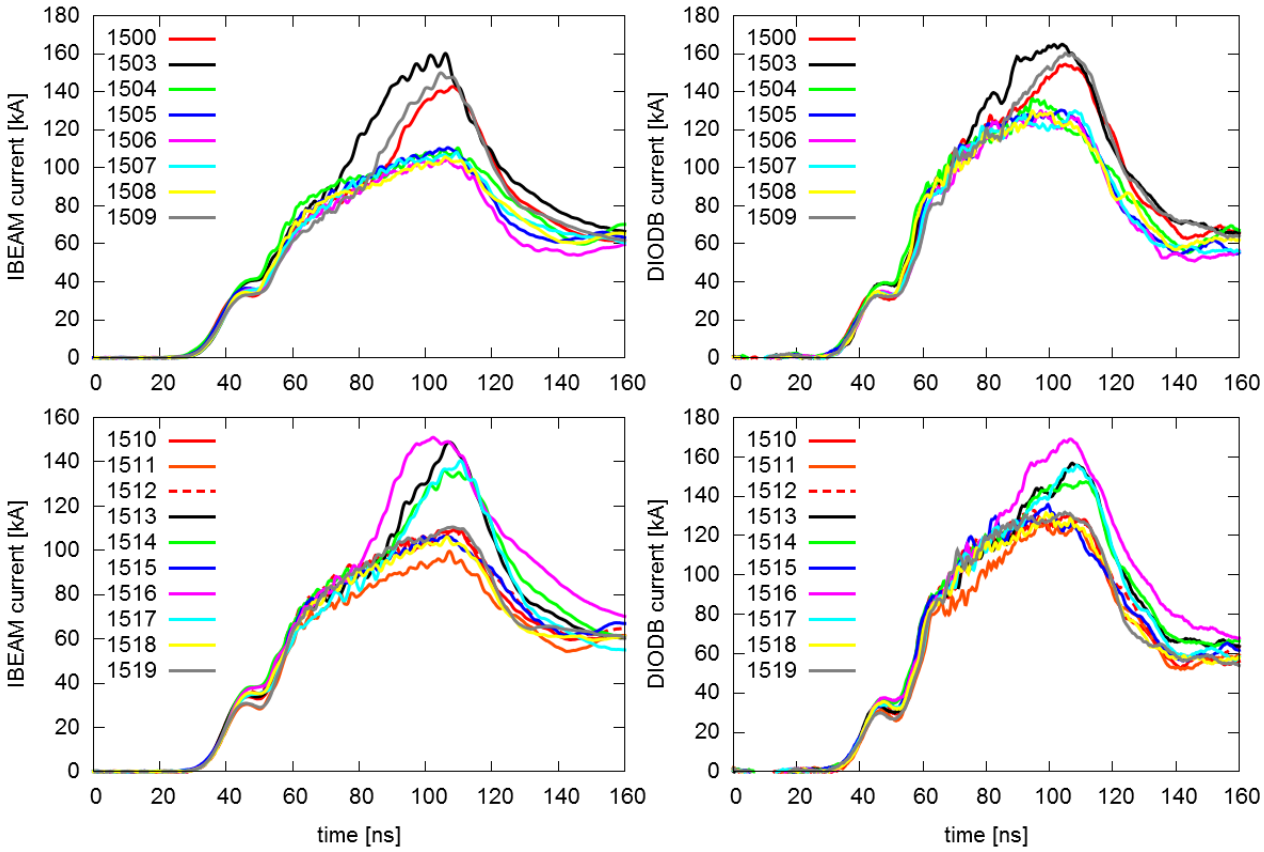

Figure 12. The IBEAM and DIODB currents from shots 1500 through 1519. All shots are 7-7.

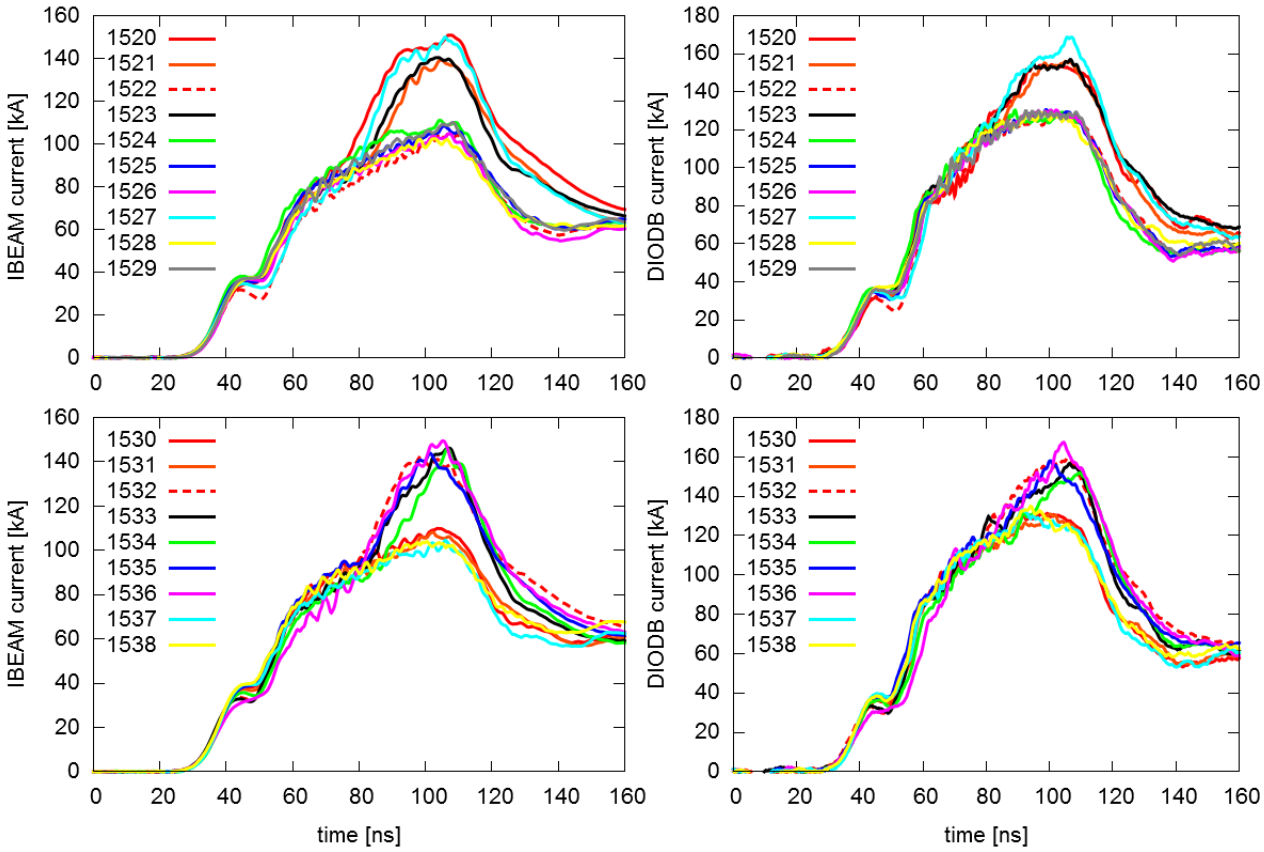

Figure 13. The IBEAM and DIODB currents from shots 1520 through 1539. All shots are 7-7.

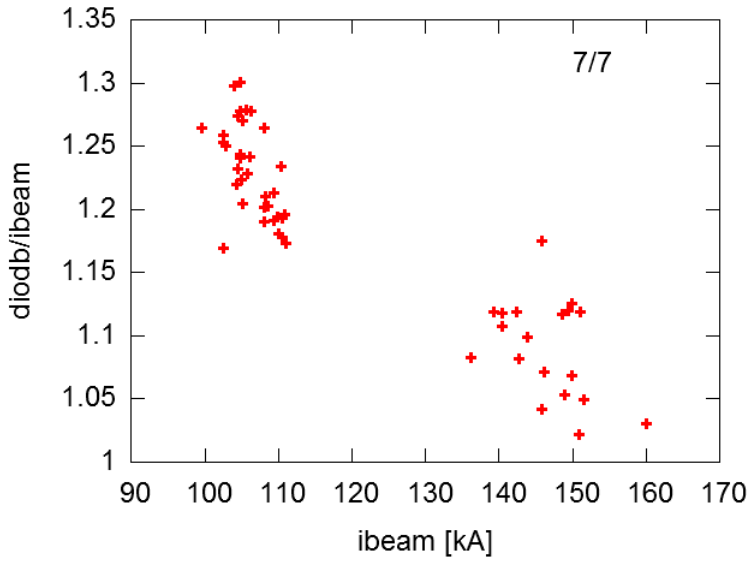

Figure 14. IBEAM versus the ratio DIODB/IBEAM from 53 *7-7* shots. The peak currents are used.)

8 Diode current comparison to theory

The SMP diode operates as a current-limited device, in which the critical current is given by [3, 5]

$$I_{crit} = 8.5\alpha \frac{r_C}{g}(\gamma^2 - 1)^{1/2} \quad \text{[kA]}, \tag{1}$$

where $\gamma = 1 + eV/m_e c^2$, r_C is the cathode radius, g is the AK gap width, and α is a scale factor used to account for the current increase due to ion space-charge. Estimates of α range from 1.6 to 2.8, depending on the diode geometry and the beam and ion space-charge profiles. Therefore, Eq. 1 includes bipolar flow, but does not include the effects of evolving plasmas as described in Ref. 2. Two plasma-related effects were identified which decrease the diode impedance during operation. The first is an expanding anode plasma, which continually reduces the effective g and occurs in normal diode operation. The second is an increased ion space-charge around the cathode needle, which would rapidly increase α when it occurs.

Equation 1 indicates that diodes with the same r_C/g will have the same impedance. This should be seen in comparisons of IBEAM (I_{crit}) early in the pulse for shots at the same voltage (γ). However, since the plasma expansion rate is a function of the diode voltage, the rate of gap closure, $g(t)$), will be the same for all shots. Therefore the ratio $r_C/g(t)$ will change differently. If we denote the plasma expansion velocity as v_p, the gap closure rate can be modeled simply as $g(t) = g_0 - v_p t$. Then

$$I_{crit}(t) = I_{crit}(0)\frac{g_0}{g_0 - v_p t}, \tag{2}$$

independent of r_C, for constant γ.

To recover the equivalence of shots with identical r_C/g, but different g, the diode impedance can be plotted on a scaled time axis using

$$I_{crit}(t') = I_0(\frac{1}{1 - v_p t'}), \tag{3}$$

where $t/g_0 \rightarrow t'$, assuming γ is constant, or

$$Z_{diode}(t') = Z_0(1 - v_p t'), \tag{4}$$

if it is not.

Simulation results for $Z_{diode}(t')$ are plotted in Fig. 15, which compares an 8.5-mm-diameter cathode to a 12.5-mm cathode, both with $r_C/g_0 = 2$. Expanding anode plasmas are included in the model.

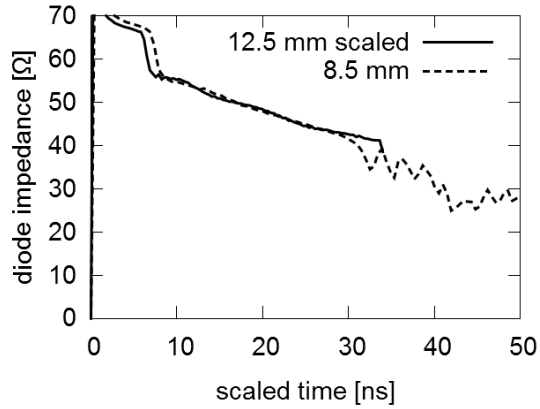

Figure 15. The diode impedance from simulations of 8.5 and 12.5-mm diameter cathodes on a scaled time axis. (For the 12.5-mm cathode, $t \rightarrow 8.5/12.5\ t$.) The simulations include effects of expanding anode plasmas.

Measurement results for $I_{crit}(t')$ are shown in Fig. 16. The diode currents from three random shots, a *6-6*, *7-7*, and *8-8*, are compared. $\gamma(t)$ is assumed to be a similar function for each shot. Figure 16a shows IBEAM currents on an unscaled time axis, while Fig. 16b shows the same data with $t' = t/g_0$.

Since the scaling of Eq. 3 holds for simulation and data, we can determine the value of v_p. In Fig. 17, Eq. 1 is plotted over IBEAM from shot 1441, using $v_p = 1$ cm/μs, $\alpha = 1.1$, and $\gamma(t) = 8 + 0.0625t$, where t is in ns. The form of $\gamma(t)$ is estimated from the simulation in Sec. 3.3. We see that the v_p used in the massive-electron-model and Eq. 1 are the same.

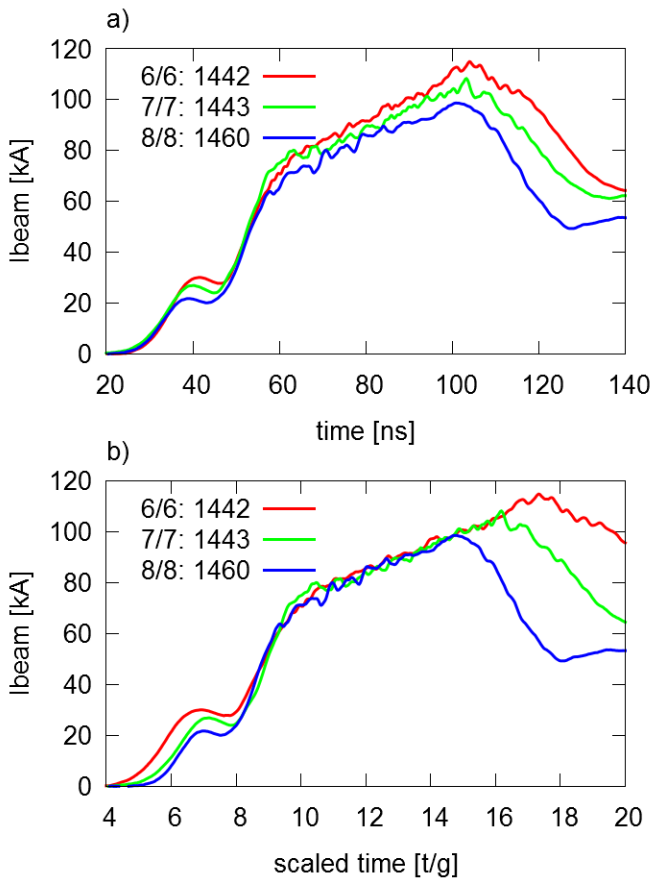

Figure 16. a) The IBEAM diode currents from shots 1442, 1443, and 1460, which are 6-6, 7-7, and 8-8 configurations, respectively. b) The same IBEAM currents with the time axes scaled by $t' = t/g_0$.

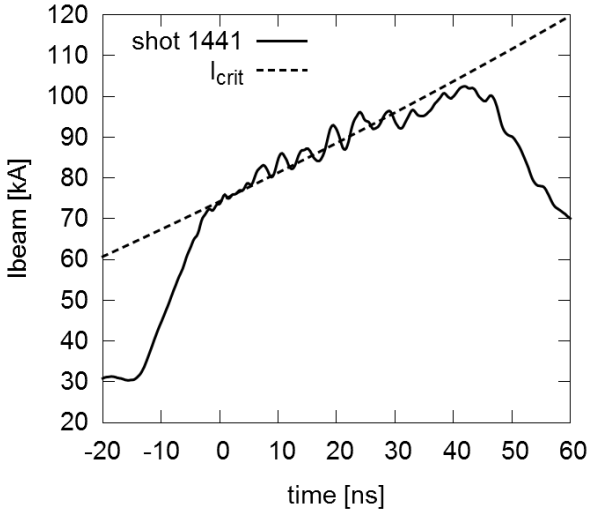

Figure 17. Theoretical critical current and IBEAM for a time-dependent AK gap. Equation 1 using $v = 1$ cm/μs, $\alpha = 1.1$, and $\gamma(t) = 8 + 0.0625t$ where t is in ns. The time axis has been shifted.

9 Conclusion

The recent experimental campaign conducted on Sandia's RITS-6 accelerator was used to improve understanding of the shot-to-shot variation of the SMP diode. The accelerator was operated at 4.5 MV which simplified the analysis by removing the variability introduced by knob emission.

In this report, we examined sources of variability which occur away from the diode, specifically

- power flow emission and trajectory changes,
- variations in pulsed power amplitude,
- variations in pulse rise,
- dustbin and transmission line misalignment, and
- different knob shapes.

Simulations of the transmission line, dustbin, and diode showed consistent power-flow electron emission and trajectories. Statistical analyses of peak power, pulse rise, asymmetries in IFEED, and asymmetries in IF show no correlation with poor radiographic shots. Lastly, one of the six knobs used has a higher occurrence of shot failure, however failures occur for every knob. We find no sources of accelerator variation which are associated with poor radiographic performance.

Shots which perform well radiographically are well-described by the theoretical critical current equation in which we use a time-dependent AK gap width. The estimated gap closure velocity is approximately $v_p = 1$ cm/μs.

In classifying good versus poor shots, we find that there is not a continuous spectrum of diode impedance behavior but that the good and poor shots can be grouped into two distinct impedance profiles. This result will form the basis of a follow-on study focusing on the variability resulting from diode parameters and beam and plasma physics.

References

[1] J.R. Threadgold, I. Crotch, D.V. Rose, and J. Maenchen. 2-D LSP simulations of the self magnetic pinch diode. In *Proc. of the* 14th *IEEE International Pulsed Power Conference*, page 995. IEEE, 2003.

[2] Nichelle Bruner, Dale R. Welch, Kelly D. Hahn, and Bryan V. Oliver. Anode plasma dynamics in the self-magnetic-pinch diode. *Phys. Rev. ST Accel. Beams*, 14(2):024401, Feb 2011.

[3] S.B. Swanekamp, G. Cooperstein, J.W. Schumer, D. Mosher, F.C. Young, P.F.Ottinger, and R.J Commisso. Evaluation of self-magnetically pinched diodes up to 10 MV as high-resolution flash X-ray sources. *IEEE Trans. Plasma Sci.*, 32:2004, 2004.

[4] D.V. Rose, D. R. Welch, B. V. Oliver, R. E. Clark, D. L. Johnson, J. E. Maenchen, P. R. Menge, C. L. Olson, and D. C. Rovang. Coupled particle-in-cell and Monte Carlo transport modeling of intense radiographic sources. *J. Appl. Phys.*, 91:3328, 2002.

[5] B. V. Oliver, K. D. Hahn, M. D. Johnston, and S. Portillo. Advances in high intensity e-beam diode development for flash x-ray radiography. *Acta Phys. Pol. A*, 115:1044, 2009.

DISTRIBUTION:

1 Voss Scientific, LLC
Attn: Dale R. Welch
418 Washington St SE
Albuquerque, NM 87108

1 MS 0899 Technical Library, 9536 (electronic copy)

Sandia National Laboratories